Journal of the Korean Physical Society, Vol. 74, No. 2, January 2019, pp. 94∼97

Fabrication of Si-based AFM Probe with High Q-factor for Fast Non-Contact Mode Scanning

Sebin Bahn and Soo Bong Choi*
Department of Physics, Incheon National University, Incheon 22012, Korea

Woongkyu Park
Department of Physics and Astronomy and Center for Atom Scale Electromagnetism, Seoul National University, Seoul 08826, Korea

Hae-Yong Jeong and Kyung-Ho Park
Nanodevices Lab, Device Technology Division, Korea Advanced Nano fab Center, Suwon 16229, Korea

(Received 18 August 2018)

In non-contact atomic force microscopy, a feedback loop is used to maintain the set-point frequency relative to the force between the specimen and the cantilever. The quality factor of the cantilever affects the sensitivity of feedback loop. Therefore, the fabrication of a high-quality-factor cantilever to improve the scan speed of non-contact atomic force microscopy is highly desirable. Here, we optimized the thickness of the non-contact atomic force microscope's cantilever to maximize the quality factor with a high resonant frequency. These maximized values reached about 1200 and 530 kHz, respectively. The corresponding scan rate was more than 0.12 mm/s, indicating that the cantilever can be used in high-speed non-contact atomic force microscopy.

PACS numbers: 46.70.De, 45.20.dg, 62.40.+I, 07.79.Lh
Keywords: NC-AFM, High Q-factor, Fast speed scan, High resonant frequency
DOI: 10.3938/jkps.74.94

I. INTRODUCTION

Recent research on semiconductor and micro-electromechanical systems (MEMS) technologies have led to high demands for miniaturization of devices for better energy efficiency and fast functionality. Many researchers and engineers have used a microscope to observe the microscopic world, but the observations of micro-nanometer-scale devices are limited due to the limitation of each microscope. A high-resolution microscope is required to achieve and inspect high-performance MEMS devices. In the case of an optical microscope, which is commonly used, the spatial resolution is restricted by the diffraction limit of light. The electron microscope has a problem of damaging the specimen due to its high voltage. Another problem is that an electron microscope can only acquire images of conducting materials.

On the other hand, non-contact atomic force microscopy (NC-AFM), which is a kind of scanning probe microscope (SPM), is a powerful tool for obtaining high-resolution topography images with minimal damage to the sample. NC-AFM uses a feedback loop that keeps the attractive force between the tip and the sample at a constant value by maintaining the set-point frequency (resonant frequency). In the feedback loop, the sensitivity and the response time are related to a quality factor (Q-factor) and the resonant frequency of the cantilever. For these reasons, a high Q-factor and a high resonant frequency are very important factors in applying the fast scan mode to a NC-AFM system [1]. In this research, we made a cantilever with a high Q-factor and a high resonant frequency. We optimized the geometrical factor (the length or thickness) of the cantilever, and we obtained the probes with Q-factors at least 2 to 4 times higher than that of a commercial NC-AFM probe ('Nanoworld', NCHR). We also investigated the relationship between the maximum scan speed on the NC-AFM system and the maximum Q-factor or the resonant frequency.

II. Q-FACTOR CALCULATIONS

Before fabricating the cantilever with a high Q-factor and a high resonant frequency, we needed to determine

*E-mail: sbchoi@inu.ac.kr

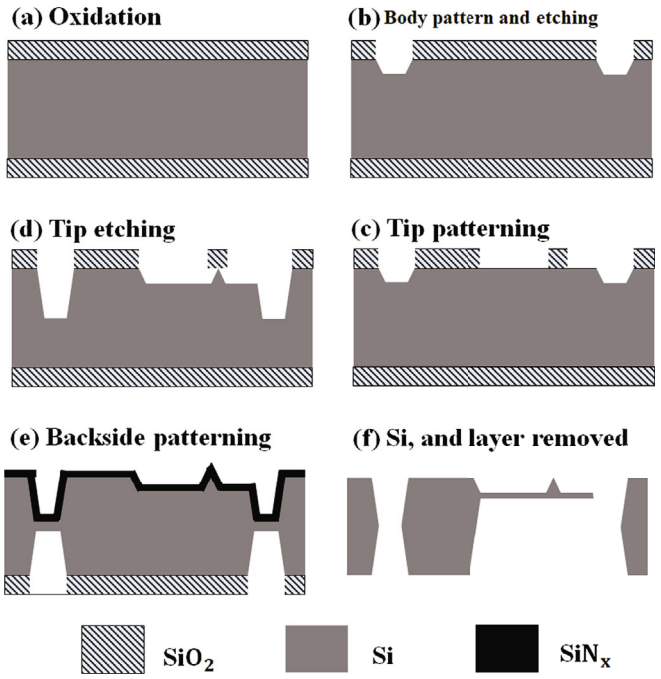

Fig. 1. Schematic diagram for the fabrication of the NC-AFM probe.

the optimal geometric conditions - the length, width, and thickness. To do this, we had to calculate the theoretical total Q-factor, which correlates to a drag force and the damping of a system such as the oscillatory motion of a sphere in a viscous fluid, which can be explained by using the Landau and Lifshitz equation [2,3]. Generally, the total Q-factor is closely connected with the energy dissipation of the system during forced oscillation. Because this relation is not expressed in a linear form, we need to identify the exact relationship between the drag force and the energy dissipation of the system. The total Q-factor can be calculated in many ways. Here, we propose a first-principles calculation of the total Q-factor by using the drag force model. To obtain the total Q-factor, we divide the total energy, which is stored in the cantilever for NC-AFM, by the energy dissipation term. Each of the Q-factors, which can be calculated and expressed with the thickness and the length of the cantilever, has its own energy dissipation term so that the total Q-factor is expressed as the sum of reciprocals of each Q-factor. ($\frac{1}{Q_{\mathrm{T}}} = \frac{1}{Q_1} + \frac{1}{Q_2} + \frac{1}{Q_3} + \frac{1}{Q_4} \cdots$, where the '$Q_{\mathrm{T}}$' is the total Q-factor and 'Q_1', 'Q_2' ... are the Q-factors of each cantilevers.). By calculating the total Q-factor, we can optimize the length and the thickness of the cantilever for the maximum Q-factor, which is proportional to the thickness and to the reciprocal of the square of the length. By using both equations (the resonant frequency and the maximum Q-factor point), we can obtain the optimal thickness of the cantilever so that it has the maximum Q-factor with a high resonant frequency.

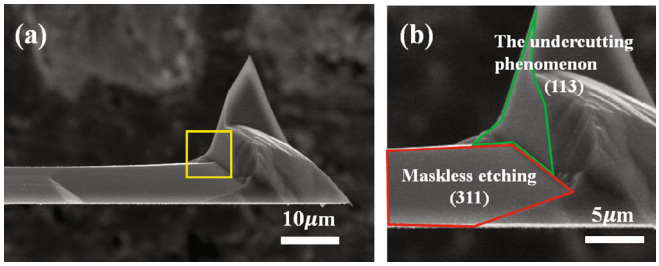

Fig. 2. (Color online) (a) SEM images of the fabricated probe, and of the (b) etched surface mismatch, which comes from the maskless and the mask etchings with the undercutting phenomenon.

III. CANTILEVER PREPARATION

Schematics of the fabrication process for the NC-AFM probe are presented in Fig. 1. Before the dry etching process for cantilever patterning, we made an oxide etch mask layer (1 μm) to discriminate the body, the cantilever and the tip area (Fig. 1(a)). At first, the body pattern was made of an oxide layer fabricated by using a reactive ion etching process (RIE). After that, we etched the silicon area with potassium hydroxide (KOH) for the anisotropic etching process (Fig. 1(b)). The depth of the etched silicon was related to the thickness of the cantilever. This target could be realized after the backside etching process. The second step was patterning the tip mask by using photolithography and the RIE technique (Fig. 1(c)). In the tip mask formation, the mask edge line was designed in consideration of the undercutting phenomenon [4]. Worthy of note is that the cantilever mask length should be longer than the target length, considering the decrease in the total length due to the undercutting phenomenon. The third step was the tip etching process (Fig. 1(d)). In this step, we needed to consider the angle difference between the (100) surface and the etched surface at maskless - anisotropic etching [5, 6]. For the anisotropic etching process, the tip shape was formed by the (113) planes according to the shape of the mask pattern and had an angle of 72° with the wafer's (100) surface [4]. The anisotropic etching process determined the direction of the etched surface based on the crystal structure of silicon [7]. If we neglect the undercutting phenomenon, the angle difference with an etched surface and the silicon wafer surface is set to 54.76° and the etching pattern will be determined by the shape of the mask and the silicon wafer's direction [8,9]. For the maskless - etching case, however, the etch rate at the etched surface will be different due to changes in the crystal plane's direction, which affects the anisotropic etching process [6]. Controling the thickness of cantilever without an etch stop layer by confirming the width of the etched surface is important. The backside etching proceeded after coating on the front side with low-stress silicon nitride (SiN_x) and silicon oxide (SiO_2) (Fig. 1(e)). Finally, after the backside etching was com-

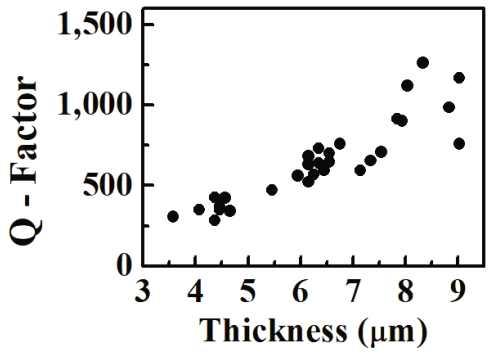

Fig. 3. Graph of the thickness dependence of Q-factor (4 ∼ 10 μm).

pleted, the process was finished by removing the front side coating (Fig. 1(f)).

Figure 2(a) shows SEM images of the fabricated tip. This form was set by using maskless and mask etching with the undercutting phenomenon (Figs. 1(c) and (d)). In Fig. 2(b), we can see that the etched surface's crystal direction is mismatched at the boundary of the tip and the cantilever bar due to the mask (tip) and maskless (cantilever bar) etching processes.

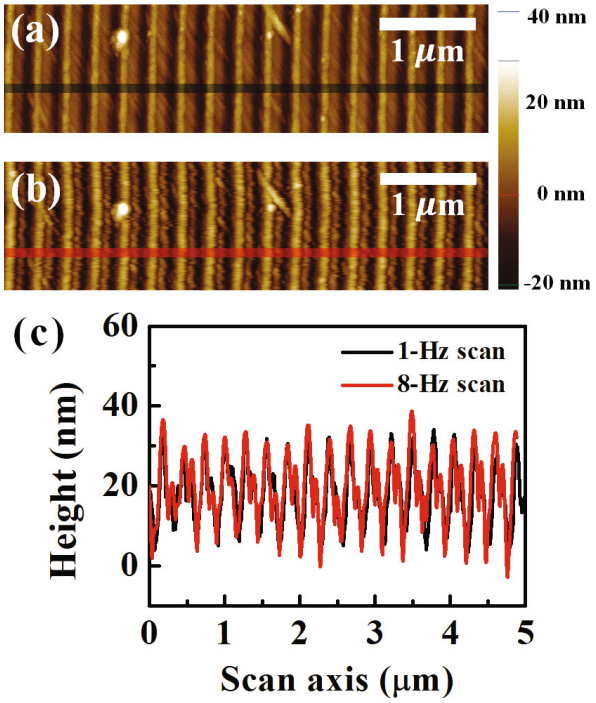

Fig. 4. (Color online) Topography with the NCHR probe at (a) a low scan rate (1 Hz) and (b) a high scan rate (8 Hz - scan speed limit). (c) Comparison of the topography data on fast NC-AFM scanning for scan rates of 1 and 8 Hz.

IV. EXPERIMENTS RESULTS

After the fabrication, we conducted the experiments and analyzed the performances of cantilevers from two perspectives. The first is to confirm the theoretical maximum Q-factor point by comparing the theoretical and the experimental thickness values. The second is to identify the limitation of the scan speed, which was that increased by the improvements in the Q-factor and the resonant frequency.

First, we investigated the effect of the thickness of the cantilever on the change in the Q-factor. That the Q-factor is affected by the ratio between the thickness and the length of the cantilever is well known [3]. The result in the Ref. 3 suggests that the Q-factor can't infinitely increase as the cantilever's thickness is increased; a maximum point exists. In the 150-μm-length case, the theoretical calculation showed a maximum Q-factor at a thickness around 8 μm. Thus, we tried to find the maximum value of the Q-factor by fixing the cantilever length at 150 m and changing the thickness from 4 μm to 13 μm. We found that the maximum Q-factor occurred near a cantilever thickness of 8.4 μm. The Q-factor was more than 1200, which was much higher than that of 4-μm-thickness sample having a Q-factor value around 300 ∼ 400 (Fig. 3). The resonant frequency is also related to the thickness and the length of the cantilever. If we fix the length, the resonant frequency will be proportional to the thickness of the cantilever:

$$f_0 = 0.162 \cdot \sqrt{\frac{E}{\rho}} \cdot \frac{t}{L^2} \ , \tag{1}$$

where E is Young's modulus, ρ is the density, t is the thickness and L is the length. The fabricated cantilever with a thickness of 4 μm to 13 μm exhibited a resonant frequency band from about 230 kHz to 800 kHz. The thickness dependence of the Q-factor was investigated at frequencies to about 600 kHz (Thickness: ∼ 9 μm) because of the frequency sweep limit in the non-contact AFM system (Park System, XE 100 series).

Second, to investigate the effect of the Q-factor and the resonant frequency on the fast scan mode, we measured a grating sample with a pitch size of ∼ 280 nm and a depth of 50 nm or more at the same position by using a commercial probe (Nanoworld Corp, NCHR) and the fabricated probe. We scanned the same interval (5 μm length along the scan axis) at various scan rates from low rate (1 Hz) to a high rate to define a limit on the scan speed of each probe (Figs. 4(a) and (b)). The 'NCHR' probe case, which had Q-factor of 350 and a resonant frequency of 270 kHz, showed a scan rate limit at 8 Hz with a depth measurement value shallower than that on the sample spec sheet data (Fig. 4(c)). On the other hand, the fabricated probe with a higher resonant frequency (351 kHz) and Q-factor (600.75) showed topography image (Figs. 5(a) and (b)) at a 12-Hz sample rate without

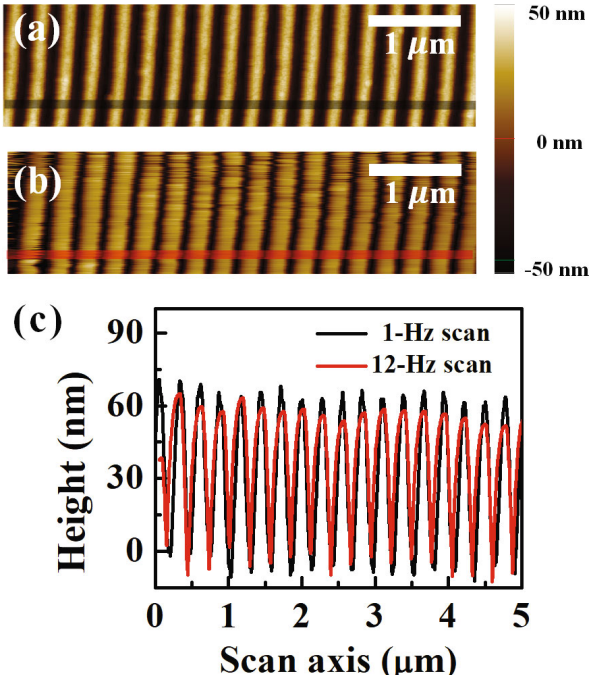

Fig. 5. (Color online) Topography with the fabricated probe at (a) a low scan rate (1 Hz) and (b) a high scan rate (12 Hz - scan speed limit). (c) Comparison of the topography data on fast NC-AFM scanning for scan rates of 1 and 12 Hz.

any distortion or mismatch of the pitch size (Fig. 5(c)). In this case, the measured depth was higher than 50 nm with the topology graph being much clearer than the one obtained by using the NCHR probe. The speed in the high Q-factor probe scan can be seen to be improved by 50% compared to the previous scan, even though the resonant frequency is increased. From this, we can see that the scan speed can be increased not only by increasing the resonant frequency but also by using a high Q-factor, which affects the sensitivity and the response speed at the feedback loop.

As a result of the above, we were able to adjust the resonant frequency and the Q-factor by controlling the ratio between the length and the thickness of the cantilever. The resonant frequency was found to have a sufficiently high value corresponding to the maximum point of the Q-factor. Therefore, by matching the maximum point of each parameter, we find and utilize the maximum scan speed for the fast scan mode. Also, we used the fast scan mode with the fabricated probe at a 12-Hz sample rate and 10-μm scan size (forward and backward); the corresponding speed was 0.12 mm/s.

V. CONCLUSION

We have investigated the resonant-frequency responses of a cantilever by considering the correlation between the thickness and the length to find the maximum Q-factor. As the cantilever thickness was increased for given length of 150 μm, the Q-factor showed a maximum at around 8.4 μm, and the resonant frequency increased in proportion to the thickness of the cantilever. The scan speed was improved from 8 Hz to 12 Hz, a 50% increase. From this result, we can conclude that the scan speed was affected not only by the resonant frequency band but also by the Q-factor.

ACKNOWLEDGMENTS

This research was supported by an Incheon National University research grant in 2016.

REFERENCES

[1] S. Hosaka, K. Etoh, A. Kikukawa and H. Koyanagi, J. Vac. Sci. & Tech. B **18**, 94 (2000).
[2] F. R. Blom, S. Bouwstra, M. Elwenspoek and J. H. J. Fluitman, J. Vac. Sci. & Tech. B **10**, 19 (1992).
[3] K. Naeli and O. Brand, J. App. Phys. **105**, 014908 (2009).
[4] D. P. Burt, P. S. Dobson, L. Donaldson and J. M. R. Weaver, Microelect. Engin. **85**, 625 (2008).
[5] X. Li, M. Bao and S. Shen, Sensors and Actuators A **57**, 47 (1996).
[6] J. Han, X. Li, H. Bao, G. Zuo, Y. Wang, F. Feng, Z. Yu and X. Ge, J. Micromech. Microeng. **16**, 198 (2006).
[7] G. T. A. Kovacs, N. I. Maluf and K. E. Petersen, IEEE. **86**, 1536 (1998).
[8] I. Barycka and I. Zubel, Sensors and Actuators A **48**, 229 (1995).
[9] C. Liu, *Foundations of MEMS* (Prentice Hall, NJ, 2005), p. 351.